An Energetic Wave Equation for Modelling Diffuse Sound Fields - Application to Open Offices

Hugo Dujourdy, Baptiste Pialot, Thomas Toulemonde, Jean-Dominique Polack

An Energetic Wave Equation for Modelling Diffuse Sound Fields - Application to Open Offices

Hugo Dujourdy[1,2], Baptiste Pialot[1],
Thomas Toulemonde[2], Jean-Dominique Polack[1]

[1] Sorbonne Université, CNRS, Institut Jean Le Rond d'Alembert, F-75005 Paris, France.
[2] Impédance S.A.S., 80 domaine de Montvoisin, 91400 Gometz-la-ville, France.
jean-dominique.polack@sorbonne-universite.fr

Abstract

By revisiting the relationships between energy density and sound intensity, this paper presents an energetic wave equation adapted for flat rooms such as open offices. We introduce the theory of the stress-energy tensor in the two-dimensional case. We derive a two-dimensional linear, second-order, hyperbolic equation that depends on few parameters such as mean free path, absorption and scattering coefficients. We solve it by a finite difference technique in the time domain and compare the results with in situ measurements to find appropriate values of the model parameters by an adjustment procedure. Results show fair agreement with measurements in the case of diffusing open spaces.

Keywords: *architectural acoustic, energy density, wave equation, scattering coefficient, room acoustic modelling, in situ measurement, SoundField microphone.*

1 Introduction

The first scientific treatment of room acoustics is generally credited to W.C Sabine, who, in 1894, empirically derived the laws of reverberation when trying to improve the acoustics of the former lecture theatre in the Fogg Art Museum at Harvard [1]. He discovered that sound energy decreases exponentially with time, and that the logarithmic decay rate is directly proportional to the area of absorbing materials present in the room. Later, he derived a theoretical model to explain his experimental founding, basing it on the so-called diffuse field approximation: in steady state, sound energy is uniformly distributed in a room, and flows in all directions isotropically.

With time, many researchers reported discrepancies between Sabine's model and measurements. Many of them attempted to improve Sabine's reverberation theory, but strangely enough, very few challenged the root of this theory, the diffuse field approximation, even though everyday experience shows that energy is not uniformly distributed in real sound fields. Thus Bosquet [2] was able to explain the paradox of absorption coefficients larger than unity by the non-uniform distribution of energy; and ISO 14257:2001 standard [3] recommended to measure the energy decay with distance, instead of the reverberation time, to characterize industrial halls, following a path laid a decade before by several national regulations, such as the French one [4]. Ollendorff [5] was the first to propose a model for a non-uniform distribution of sound energy in disproportionate rooms, but his diffusion model escaped notice until it was rediscovered by Picaut et al. some 20 years later [6]. Beside the traditional absorption coefficient introduced by Sabine to characterize the materials on the walls, the diffusion model introduces a diffusion coefficient within the room. But all attempts to measure the diffusion coefficients have failed so far [7].

In order to overcome this difficulty, Dujourdy et al. [8] revisited the original derivation of the diffusion equation by Morse and Feshbach [9]. They realized that, beside the usual conservation of the total energy used by Bosquet, Morse and Ingard [10] introduced a second conservation equation, the conservation of sound intensity, and combined the two equations in the covariant conservation of a single tensor, the stress-energy tensor. Dujourdy et al. supplemented these conservation equations by an energy and momentum balance on the walls that allowed them to introduce absorption and scattering coefficients in the equations, the former being the usual absorption coefficient. They transformed this system in a one-dimensional Telegraph equation involving energy only, and solved

it by using a finite difference scheme. Results showed that only the smaller of the two absorption and scattering coefficients pilots the time decay rate, allowing to evaluate them sequentially from an initial guess: the smaller coefficient from the time decay curves; and the larger from the space decay curves. The procedure permits the evaluation of locally varying absorption and scattering.

In the present paper, we apply the theory developed by Dujourdy et al. [8] for one-dimensional spaces to two-dimensional spaces such as open offices. Integrating on the smallest dimension of a flat room lets us obtain a two-dimensional equation well suited for spaces such as open offices. After a short presentation of Sabine's and Ollendorff-Picaut's models (Sec. 2), we recall Dujourdy's model and develop it in the two-dimensional case, including the energy and momentum balance on the floor and the ceiling (Sec. 3). We obtain a linear, second order, hyperbolic, differential equation for the energy density, which we then solve (Sec. 4) with a finite difference time domain (FDTD) method. We chose an explicit and fast-computing, two-dimensional algorithm with mixed boundary conditions. In Sec. 5 we validate the two-dimensional model and compare the results with *in situ* measurements. Sec. 6 discusses the results and Sec. 7 concludes the paper.

2 State of the art

2.1 Bosquet's synthetic theory of reverberation

All theories of reverberation are more or less based on Bosquet's synthetic theory of reverberation [2], that simply expresses the conservation of energy in space. It therefore takes two forms:

- a *local form*: $\partial_t w + \vec{\nabla} \cdot \vec{I} = \Pi$
- a *global form*, by spatial integration of the local form over the volume V bounded by surface S:

$$d_t \int_V w dV + \int_S \vec{I} \cdot \vec{n} dS = \Pi \tag{1}$$

where ∂_t is the partial derivative and d_t the total derivative with respect to time, $\vec{\nabla}\cdot$ is the divergence operator, w the total instantaneous sound energy density, $\vec{I}$ the sound intensity vector, $\vec{n}$ the outbound normal vector, and Π the power of the sound source which is considered localized at a single position. Reverberation theories differ in the relationship that links sound intensity to the total instantaneous sound energy density. Notice, however, that in the global form, the second term on the left hand side of Eq. (1) only considers the intensity penetrating the boundaries, that is, the absorbed energy flow.

2.2 Sabine's model

As stated in the Introduction, Sabine's model assumes uniform distribution of the sound energy within space, and isotropic distribution of its flow in all directions: the so-called diffuse field approximation. Thus, the relationship between sound intensity in *each direction* and the total instantaneous energy density w, considered to be independent of position in the room, is simply given by:

$$|\vec{I}| = \frac{w}{4\pi} c$$

where c is the speed of sound. Traditionally, one singles out on the boundaries the incident intensity by summing the energy flow given by the preceding equation only on the directions impinging on the boundaries. The total incident energy on the boundaries is thus:

$$\int_S \vec{I}_i \cdot \vec{n} dS = \frac{w}{4} cS$$

Taking into account that only a fraction of the incident energy is absorbed by the boundaries, Eq. (1) thus becomes:

$$V \partial_t w + \frac{\bar{\alpha} S c}{4} w = \Pi \tag{2}$$

where we have introduced the mean absorption coefficient $\bar{\alpha}$ on the boundaries. After the sound source has been turned off, $\Pi = 0$ and it is obvious from Eq. (2) that sound energy decays exponentially with time and with decay rate $\frac{\bar{\alpha}Sc}{4V}$.

However, as stated by Polack [11], the diffuse field approximation is incompatible with any absorption on the boundaries, as in such cases energy flows from the source to the boundaries, in contradiction with an isotropic flow of energy in all directions. Nevertheless, despite this major shortcoming, the diffuse field approximation proves very useful in architectural acoustics, as long as it is used in proportionate spaces, that is, in spaces where no dimension is much larger or smaller than the other two.

2.3 Ollendorff-Picaut's model

Ollendorf [5], followed by Picaut et al. [6], proposed a different type of relationship between sound intensity and mean energy. Assuming that sound energy flows from regions of high energy density, such as the source, to regions of low energy density, such as the absorbing walls, they proposed that the sound intensity be negatively proportional to the sound energy *gradient*, following a suggestion by Morse and Feshbach [9]:

$$\vec{I} = -\delta\vec{\nabla}w$$

where $\vec{\nabla}$ is the gradient operator and δ the diffusion coefficient. In this case, local energy conservation simply reduces to a diffusion equation:

$$\partial_t w - \delta\Delta w = \Pi$$

where Δ is the Laplacian operator. If one "renormalizes" the absorption by introducing a constant decay rate σ within the volume as proposed by Picaut et al. [6], one obtains a modified diffusion equation:

$$\partial_t w + \sigma w - \delta\Delta w = \Pi$$

After the sound source has been turned off, this equation admits an analytical solution in infinite space:

$$w(\vec{r},t) = \frac{1}{(4\pi\delta t)^{\frac{d}{2}}}\exp\{-\frac{r^2}{4\delta t} - \sigma t\}$$

where d is the space dimension. In flat ($d = 2$) or narrow ($d = 1$) spaces, it can readily be shown that $\sigma = \frac{\bar{\alpha}Sc}{4V}$, which can be generalised to bounded three-dimensional spaces using probabilistic considerations [6]. That is to say, energy eventually decreases exponentially with time and with the same decay rate as in the diffuse field approximation.

However, the main feature of Ollendorff-Picaut's model is a non-uniform distribution of the steady-state sound energy: as one moves away from the source, the sound energy decreases, as stated in ISO 14257 [3].

3 Theory

3.1 Energy and intensity conservation

Following Morse and Feshbach [9], we define the instantaneous energy density E as:

$$E = \frac{\rho}{2}(\frac{1}{c^2}|\partial_t\Psi|^2 + |\vec{\nabla}\Psi|^2) \tag{3}$$

and the sound intensity vector $\vec{I}$ as:

$$\vec{I} = -\rho\partial_t\Psi\vec{\nabla}\Psi$$

where ρ is the air density, and Ψ the velocity potential from which the particle velocity and the sound pressure are defined by $\vec{v} = -\vec{\nabla}\Psi$ and $p = \rho\partial_t\Psi$ respectively. In the following, we denote ∂_i and ∂_{ii} the first and second derivatives according to coordinate i.

As shown in [8], following Morse and Ingard [10], a system of coupled equations for the energy density and sound intensity is obtained by multiplying the wave equation with any of the first order

derivatives of the velocity potential and applying elementary differentiation rules, leading to the conservation of sound energy and intensity. With the notation $\vec{J} = \frac{\vec{I}}{c}$, the conservation of energy is given by:

$$\frac{1}{c}\partial_t E + \vec{\nabla} \cdot \vec{J} = 0 \tag{4}$$

and the conservation of intensity by:

$$\frac{1}{c}\partial_t \vec{J} + \vec{\nabla}\underline{\underline{E}} = 0 \tag{5}$$

$\underline{\underline{E}}$ is the wave-stress symmetric tensor [10], which does not reduce to the energy density E of equation (3); but its trace remains equal to the energy density E. By extension, we still call $\vec{J}$ the sound intensity.

Developing the wave-stress tensor, Eqs. (4) and (5) are written as a system of coupled equations:

$$\begin{array}{rcl} \frac{1}{c}\partial_t E & + & \vec{\nabla} \cdot \vec{J} = 0 \\ \frac{1}{c}\partial_t \vec{J} & + & \vec{\nabla} \begin{pmatrix} E_{xx} & E_{yx} & E_{zx} \\ E_{xy} & E_{yy} & E_{zy} \\ E_{xz} & E_{yz} & E_{zz} \end{pmatrix} = 0 \end{array} \tag{6}$$

where E is given by Eq. (3) and the E_{ij} are expressed in terms of the velocity potential by:

$$\begin{aligned} E_{xx} &= \frac{\rho}{2}(\frac{1}{c^2}|\partial_t\Psi|^2 + |\partial_x\Psi|^2 - |\partial_y\Psi|^2 - |\partial_z\Psi|^2) \\ E_{yy} &= \frac{\rho}{2}(\frac{1}{c^2}|\partial_t\Psi|^2 - |\partial_x\Psi|^2 + |\partial_y\Psi|^2 - |\partial_z\Psi|^2) \\ E_{zz} &= \frac{\rho}{2}(\frac{1}{c^2}|\partial_t\Psi|^2 - |\partial_x\Psi|^2 - |\partial_y\Psi|^2 + |\partial_z\Psi|^2) \\ E_{xy} &= \rho\partial_x\Psi\partial_y\Psi \\ E_{xz} &= \rho\partial_x\Psi\partial_z\Psi \\ E_{yz} &= \rho\partial_y\Psi\partial_z\Psi \end{aligned}$$

As for the sound intensity, we note J_x, J_y and J_z its components along the three coordinates, so that $\vec{J} = (J_x, J_y, J_z) = (E_{tx}, E_{ty}, E_{tz})$. It can be also expressed in terms of the velocity potential by:

$$\begin{aligned} E_{tx} &= -\frac{\rho}{c}\partial_t\Psi\partial_x\Psi \\ E_{ty} &= -\frac{\rho}{c}\partial_t\Psi\partial_y\Psi \\ E_{tz} &= -\frac{\rho}{c}\partial_t\Psi\partial_z\Psi \end{aligned}$$

3.2 Stress-energy tensor

Equivalently, the energy quantities E, $\vec{J}$ and $\underline{\underline{E}}$ can be combined into a single tensor, the symmetric stress-energy tensor:

$$\underline{\underline{T}} = \begin{pmatrix} E & E_{tx} & E_{ty} & E_{tz} \\ E_{tx} & E_{xx} & E_{xy} & E_{xz} \\ E_{ty} & E_{xy} & E_{yy} & E_{yz} \\ E_{tz} & E_{xz} & E_{yz} & E_{zz} \end{pmatrix} = \begin{pmatrix} E & \vec{J}^T \\ \vec{J} & \underline{\underline{E}} \end{pmatrix}$$

where $(\cdot)^T$ indicates the transposed vector. The conservation of energy is simply expressed by the covariant derivative of the stress-energy tensor:

$$\vec{\nabla} \cdot \underline{\underline{T}} = 0$$

Note that the diagonal elements of the stress-energy tensor $\underline{\underline{T}}$ satisfy the relation:

$$E = E_{xx} + E_{yy} + E_{zz}$$

since kinetic and potential energies are equal everywhere in space on average.

3.3 Dimensional reduction

As in [8], dimensional reduction is obtained by integration of system (6) on the smallest spatial dimension, usually the height, taking into account the energy and momentum balance on the boundaries in terms of acoustic absorption and scattering respectively.

3.3.1 Energy balance on ceiling and floor

Starting with the first line of system (6), we consider the propagation of sound along the $\vec{x}$ and $\vec{y}$ directions in a rectangular room of dimensions $l_x \times l_y \times l_z$, where l_x is the length, l_y the width and l_z the height of the room. We assume E, J_x and J_y independent of the vertical coordinate z, strict hypotheses that can be relaxed along the lines developed in [8], and integrating along the vertical coordinate of the room:

$$\frac{1}{c}\int_z \partial_t E dz + \int_z \partial_x J_x dz + \int_z \partial_y J_y dz + \int_z \partial_z J_z dz = 0$$

we obtain the relation:

$$\frac{1}{c}\partial_t E l_z + \partial_x J_x l_z + \partial_y J_y l_z + J_z^+ - J_z^- = 0 \tag{7}$$

where J_z^+, resp. $-J_z^-$ is the energy flow through the ceiling (side $+$), resp. the floor (side $-$) of the room, that is, the sound intensity absorbed by each of them. Thus the sound intensity $J_{z,abs}$ absorbed at each instant by the ceiling or the floor at position (x, y) is:

$$J_z^+ = J_{z,abs}^+ \quad -J_z^- = J_{z,abs}^- \tag{8}$$

Simple energy balance can be introduced on each wall by considering the energy distribution function $f(\vec{r}, \vec{v}, t)$ that a sound wave at position $\vec{r}$ travels in the direction $\vec{v}$ at time t. The derivation is carried out in the Appendix, where different options are discussed, finally leading to Jing and Xiang's relation [12]:

$$J_{z,abs} = \frac{\alpha}{2(2-\alpha)}E$$

We then introduce a modified absorption coefficient A:

$$A = \frac{\alpha}{1-\frac{\alpha}{2}}$$

where $A \in [0; 1]$. Eqs. (8) become:

$$J_z^+ = J_{z,abs}^+ = \frac{A^+}{4}E \quad -J_z^- = J_{z,abs}^- = \frac{A^-}{4}E$$

and:

$$J_z^+ + \left(-J_z^-\right) = \frac{A^+ + A^-}{4}E = \frac{A}{2}E$$

where $A = (A^+ + A^-)/2$ is the mean absorption coefficient and the factor $\frac{1}{4}$ comes from the diffuse field theory (Sec. 2.2 and [13]). Eq. (7) can now be written as:

$$\frac{1}{c}\partial_t E l_z + \partial_x J_x l_z + \partial_y J_y l_z + \frac{AE}{2} = 0 \tag{9}$$

Introducing the mean free path:

$$\lambda = \frac{4V}{S} \tag{10}$$

with S the total surface area of the walls, floor and ceiling, the total surface area of a room of length l_x, width l_y and height l_z can be developed as $S = 2l_x l_y(1 + \frac{l_z}{l_x} + \frac{l_z}{l_y})$. We assume $l_y, l_x \gg l_z$. Eq. (10) becomes:

$$\lambda = 2l_z \tag{11}$$

Replacing Eq. (11) in Eq. (9), we obtain the following equation:

$$\frac{1}{c}\partial_t E + \partial_x J_x + \partial_y J_y + \frac{A}{\lambda}E = 0 \tag{12}$$

3.3.2 Momentum balance on ceiling and floor

Applying this method to the second line of system (6) leads to, for the x component of the sound intensity $\vec{J}$:

$$\frac{1}{c}\int_z \partial_t J_x dz + \int_z \partial_x E_{xx} dz + \int_z \partial_y E_{xy} dz + \int_z \partial_z E_{xz} dz = 0$$

This time, we assume J_x, E_{xx} and E_{xy} independent of the vertical coordinate, strict hypotheses that again can be relaxed along the lines developed in [8], yielding:

$$\frac{1}{c}\partial_t J_x l_z + \partial_x E_{xx} l_z + \partial_y E_{xy} l_z + E_{xz}^+ - E_{xz}^- = 0 \tag{13}$$

where E_{xz}^+, resp. $-E_{xz}^-$, is the wave stress on the ceiling (side $+$), resp. on the floor (side $-$) of the room. We postulate that this stress is equal to the sound stress momentum $M_{xz,scat}$ scattered by the ceiling or the floor:

$$E_{xz}^+ = M_{xz,scat}^+ \quad -E_{xz}^- = M_{xz,scat}^- \tag{14}$$

As for the energy balance in Sec. 3.3.1, the stress momentum balance is obtained by proper integration of the energy distribution function on the walls. The derivation is carried out in the Appendix, leading to the relation:

$$E_{xz} = \frac{3}{4}\frac{\beta}{2(2-\beta)} J_x$$

We introduce the modified scattering coefficient $D = \frac{3}{4}\frac{\beta}{1-\frac{\beta}{2}}$, and Eq. (14) becomes:

$$E_{xz}^+ = \frac{D^+}{4} J_x \quad E_{xz}^- = \frac{D^-}{4} J_x$$

and:

$$E_{xz}^+ + \left(E_{xz}^-\right) = \frac{D^+ + D^-}{4} E = \frac{D}{2} E$$

where $D = (D^+ + D^-)/2$ is the mean scattering coefficient. Thus, Eq. (13) reduces to:

$$\frac{1}{c}\partial_t J_x l_z + \partial_x E_{xx} l_z + \partial_y E_{xy} l_z + D\frac{J_x}{2} = 0 \tag{15}$$

where $D = (D^+ + D^-)/2$ is the mean scattering coefficient.

Similar methods are used for integrating the y component of the sound intensity $\vec{J}$ in the second line of system (6):

$$\frac{1}{c}\int_z \partial_t J_y dz + \int_z \partial_x E_{yx} dz + \int_z \partial_y E_{yy} dz + \int_z \partial_z E_{yz} dz = 0$$

We assume J_y and E_{yy} independent of the vertical coordinate, as $E_{yx} = E_{xy}$ is already assumed independent of z, leading to:

$$\frac{1}{c}\partial_t J_y l_z + \partial_x E_{yx} l_z + \partial_y E_{yy} l_z + E_{yz}^+ - E_{yz}^- = 0$$

and introducing the same modified scattering coefficient $D = \frac{3}{4}\frac{\beta}{1-\frac{\beta}{2}}$, we obtain a second momentum balance on the walls:

$$E_{yz}^+ = -E_{yz}^- = \frac{D}{4} J_y$$

that is:

$$\frac{1}{c}\partial_t J_y l_z + \partial_x E_{yx} l_z + \partial_y E_{yy} l_z + D\frac{J_y}{2} = 0 \tag{16}$$

We need not consider the last component of the sound intensity $\vec{J}$ in the second line of system (6), as it gives information redundant with Eq. (12).

Introducing the mean free path of Eq. (11), the two intensity conservation equations (15) and (16) combine into:

$$\frac{1}{c}\partial_t \vec{J} + \frac{D}{\lambda}\vec{J} + (\partial_x, \partial_y)\begin{pmatrix} E_{xx} & E_{yx} \\ E_{xy} & E_{yy} \end{pmatrix} = 0 \tag{17}$$

where the intensity vector $\vec{J}$ is now two-dimensional, that is, $\vec{J} = (J_x, J_y)$. Equality of kinetic and potential energies reduces to the relation $E = E_{xx} + E_{yy}$.

3.3.3 Closing the system

Eqs. (12) and (17) build up a system of coupled first order partial differential equations. Those equations describe the two-dimensional conservation of the energy density and the sound intensity, with absorption and scattering on the ceiling and floor, as functions of the modified adsorption and scattering coefficients A and D. The latter accounts for the redistribution of the directions of propagation of energy and can take values from $D = 0$, meaning that E_{xz} or $E_{yz} = 0$, to $D = +\infty$, meaning that J_x or $J_y = 0$. Contrary to absorption, the total energy is not modified in the scattering process, but only directional redistribution of the acoustic intensity takes place.

However, simple counting of variables shows that Eqs. (12) and (17) are under-determined. In the rest of the paper, we therefore postulate two further relations between the components of the wave-stress tensor $\underline{\underline{E}}$:

$$\begin{aligned} E_{xx} &= E_{yy} = \frac{E}{2} \\ E_{xy} &= E_{yx} = 0 \end{aligned}$$

amounting to equipartition of energy (first line) and decorrelation (second line), that is, to isotropic distribution of energy (diffuse field assumption). This can be simply achieved by proper scattering on the ceiling and floor of the room, as those energies are assumed independent of the vertical variable z.

In other words, contrarily to the one-dimensional case treated by Dujourdy et al. in [8], supplementary assumptions are necessary to solve the energy relations. They lead to the following form for Eq. (17):

$$\frac{1}{c}\partial_t \vec{J} + \frac{D}{\lambda}\vec{J} + \vec{\nabla}\frac{E}{2} = 0 \tag{18}$$

Besides, as in the one-dimensional case, the characteristics of the vertical side walls must also be introduced to solve the equations. They are considered as boundaries conditions in the next Section.

3.4 General equation

In one dimension, we used the similitude between Eqs. (12) and (18) and the transmission line equations to reduce the system to a single generalised wave equation involving the sound energy density. We can extend this similitude to two dimensions in order to obtain a two-dimensional generalized wave equation involving the sound energy density.

We transform Eqs. (12) and (18) as follows:

$$(\frac{1}{c}\partial_t + \frac{A}{\lambda})E = -\vec{\nabla}\cdot\vec{J} \tag{19}$$

$$(\frac{1}{c}\partial_t + \frac{D}{\lambda})\vec{J} = -\vec{\nabla}\frac{E}{2} \tag{20}$$

By differentiation of Eq. (20) with respect to space, we obtain:

$$(\frac{1}{c}\partial_t + \frac{D}{\lambda})\vec{\nabla}\cdot\vec{J} = -\Delta\frac{E}{2}$$

Replacing $\vec{\nabla} \cdot \vec{J}$ by its value in Eq. (19) yields:

$$(\frac{1}{c}\partial_t + \frac{D}{\lambda})(\frac{1}{c}\partial_t + \frac{A}{\lambda})E = \Delta\frac{E}{2}$$

which can be developed as:

$$\frac{1}{c^2}\partial_{tt}E - \Delta\frac{E}{2} + \frac{A+D}{\lambda c}\partial_t E + \frac{AD}{\lambda^2}E = 0 \tag{21}$$

Eq. (21) is a two-dimensional linear second-order hyperbolic equation. It is constituted of an ordinary wave equation, with two supplementary terms that combine the effect of absorption and scattering. Just like the one-dimensional case [8], it admits two limiting cases:

- In the *steady state* case, E does not depend on time t, and Eq. (21) reduces to:

$$\Delta\frac{E}{2} = \frac{AD}{\lambda^2}E \tag{22}$$

  with solution: $E = E_0 K_0(-\frac{\sqrt{2AD}}{\lambda}r)$, where $K_0(\cdot)$ is the modified Bessel function of second kind and E_0 a constant (initial value). The asymptotic expression of this solution is proportional to $\frac{\exp(-\frac{\sqrt{2AD}}{\lambda}r)}{\sqrt{r}}$ for large values of r [14].

- In the limit of large values of A or D, the second time derivative becomes small compared to the first one for large times t. One can neglect the second time derivative in Eq. (21), and divide it by $\frac{A+D}{\lambda}$ to obtain a *diffusion equation*:

$$\frac{1}{c}\partial_t E - \frac{\lambda}{2(A+D)}\Delta E + \frac{AD}{\lambda(A+D)}E = 0 \tag{23}$$

  with solution:

$$E = E_1\frac{e^{(-\frac{(A+D)r^2}{2\lambda ct} - \frac{ADc}{(A+D)\lambda}t)}}{t} \tag{24}$$

  where E_1 is the initial value. As Eq. (23) is not valid for small times t, solution (24) is not valid either.

Note that, when $A = D$, Eq. (21) reduces to:

$$\left(\frac{1}{c}\partial_t + \frac{A}{\lambda}\right)^2 E - \Delta\frac{E}{2} = 0$$

the solution of which is a travelling sound packet [15]:

$$E^+ = E_2 e^{(-\frac{A}{\lambda}ct)}\frac{U(\frac{c}{\sqrt{2}}t - r)}{2\pi\sqrt{(\frac{c}{\sqrt{2}}t)^2 - r^2}} \tag{25}$$

where $U(\cdot)$ is the Heaviside function and E_2 the initial value. At any position r, the overall decay is given by Sabine formula; but energy is lagging *behind* the packet front, which travels at only $\frac{1}{\sqrt{2}} \approx 0.7$ times the speed of sound, because backscattering slows down propagation.

Notice that, in all cases, absorption and scattering are fully equivalent; and that the direct sound, that is, the initial wave front, is not described by Eq. (21) nor its analytical approximations, as is further discussed in Sec. 6.2.

3.5 Conditions on the side boundaries of the room

The conditions on the side boundaries can be written from the energy balance that has been obtained earlier. With respect to the system of coupled equations, the balance gives:

$$\vec{J} \cdot \vec{n} = A_r E$$

where we remind that $\vec{n}$ is the normal vector pointing into the wall. A_r is the modified absorption coefficient applied to the side boundaries and has already been defined in the literature [12]. We have:

$$A_r = \frac{\alpha}{2(2-\alpha)} = \frac{A}{4}$$

By projecting Eq. (20) on the wall perpendicular to the $\vec{n}$ direction, we have:

$$(\frac{1}{c}\partial_t + \frac{D}{\lambda})\vec{J}\cdot\vec{n} = -\partial_n\frac{E}{2}$$

We can replace by the expression of $\vec{J}\cdot\vec{n}$ and we obtain:

$$(\frac{1}{c}\partial_t + \frac{D}{\lambda})A_r E = -\partial_n\frac{E}{2}$$

for both extremities. This reduces to the *mixed* boundary condition:

$$\partial_n\frac{E}{2} + (\frac{1}{c}\partial_t + \frac{D}{\lambda})A_r E = 0 \tag{26}$$

For rectangular rooms, n takes the values $\pm x$ or $\pm y$, depending on the side. As one can see, both the scattering coefficient D and the modified absorption coefficient A_r play a role in the boundary condition.

4 Numerical solving

In this section we present the numerical solving technique that we use to compute the general equation (21). The technique is close to the one used for the one-dimensional equation in [8] and makes use of a Finite Difference Time Domain (FDTD) method with large space and time steps compared with pressure wave equations.

4.1 Scheme

The formulation of the FDTD approximation uses a non staggered grid on energy density components. The energy density is determined at the grid positions $[i\Delta x, j\Delta y]$ and at times $n\Delta t$, with Δx and Δy the space discretization step and Δt the time discretization steps. Indices i and j mark the space points and superscript n marks the discrete times.

As in the one-dimensional case [8], we use a centred-time centred-space scheme. The approximations are:

$$\begin{aligned}
\left.\frac{\partial^2 E}{\partial t^2}\right|_x^t &= \frac{E_{i,j}^{n+1} - 2E_{i,j}^n + E_{i,j}^{n-1}}{\Delta t^2} + \mathcal{O}(\Delta t^2) \\
\left.\frac{\partial^2 E}{\partial x^2}\right|_x^t &= \frac{E_{i+1,j}^n - 2E_{i,j}^n + E_{i-1,j}^n}{\Delta x^2} + \mathcal{O}(\Delta x^2) \\
\left.\frac{\partial^2 E}{\partial y^2}\right|_y^t &= \frac{E_{i,j+1}^n - 2E_{i,j}^n + E_{i,j-1}^n}{\Delta y^2} + \mathcal{O}(\Delta y^2) \\
\left.\frac{\partial E}{\partial t}\right|_x^t &= \frac{E_{i,j}^{n+1} - E_{i,j}^{n-1}}{2\Delta t} + \mathcal{O}(\Delta t^2)
\end{aligned} \tag{27}$$

where $\mathcal{O}(\cdot)$ is the truncation error.

4.2 Discrete general equation

Replacing Eq. (27) in Eq. (21), we get:

$$\begin{aligned}\frac{E^n_{i+1,j} - 2E^n_{i,j} + E^n_{i-1,j}}{2\Delta x^2} + \frac{E^n_{i,j+1} - 2E^n_{i,j} + E^n_{i,j-1}}{2\Delta y^2} &= \frac{E^{n+1}_{i,j} - 2E^n_{i,j} + E^{n-1}_{i,j}}{c^2\Delta t^2} \\ &+ \frac{E^{n+1}_{i,j} - E^{n-1}_{i,j}}{2\Delta t}\frac{A+D}{\lambda c} \\ &+ E^n_{i,j}\frac{AD}{\lambda^2}\end{aligned}$$

that is:

$$\begin{aligned}E^{n+1}_{i,j}(a+1) &= E^{n-1}_{i,j}(a-1) + E^n_{i,j}(2 - C^2_{r_x} - C^2_{r_y} - b) \\ &+ \frac{1}{2}C^2_{r_x}(E^n_{i+1,j} + E^n_{i-1,j}) + \frac{1}{2}C^2_{r_y}(E^n_{i,j+1} + E^n_{i,j-1}) \\ &+ \mathcal{O}(\Delta t^2, \Delta x^2, \Delta y^2)\end{aligned} \tag{28}$$

with $C_{r_x} = \frac{c\Delta t}{\Delta x}$ and $C_{r_y} = \frac{c\Delta t}{\Delta y}$ the Courant-Friedrichs-Lewy coefficient for each dimension, $a = (A+D)\frac{c\Delta t}{2\lambda}$, $b = AD(\frac{c\Delta t}{\lambda})^2$. This equation is a simple explicit form of FDTD. The accuracy of this scheme is second order in time and space.

4.3 Initial and boundary equations

The initial condition corresponds to the source positioned at $\vec{r} = (x, y)$, that is, $E^0_{i,j} = 0$ except for $i\Delta x = x$ and $j\Delta y = y$ where it has a given value of $10\log E^0_{x,y} = 100$dB.

The boundary equations model the reflections on the walls. The energy balance on the boundaries is given by Eq. (26). The approximations for this equation are space and time centred:

$$\begin{aligned}\left.\frac{\partial E}{\partial x}\right|^t_x &= \frac{E^n_{i+1,j} - E^n_{i-1,j}}{2\Delta x} + \mathcal{O}(\Delta x^2) \\ \left.\frac{\partial E}{\partial y}\right|^t_y &= \frac{E^n_{i,j+1} - E^n_{i,j-1}}{2\Delta y} + \mathcal{O}(\Delta y^2) \\ \left.\frac{\partial E}{\partial t}\right|^t_x &= \frac{E^{n+1}_{i,j} - E^{n-1}_{i,j}}{2\Delta t} + \mathcal{O}(\Delta t^2)\end{aligned}$$

Those approximations are introduced in Eq. (26) to obtain discrete boundary equations which are then used to replace the undefined boundary terms in Eq. (28). We separately consider the extremities $x = 0$, $y = 0$, $x = l_x$ and $y = l_y$, respectively characterized by index values $i = 1$, $j = 1$, $i = l_x/\Delta x$, and $j = l_y/\Delta y$:

$$\begin{aligned}E^{n+1}_{1,j}(1 + a + A_r C_{r_x}) &= E^n_{1,j}(2 - (C^2_{r_x} + C^2_{r_y}) - b - 2C^2_{r_x}\sigma_x) + C^2_{r_x}E^n_{2,j} \\ &+ \frac{1}{2}C^2_{r_y}(E^n_{1,j+1} + E^n_{1,j-1}) + E^{n-1}_{1,j}(a - 1 + A_r C_{r_x}) \\ E^{n+1}_{i,1}(1 + a + A_r C_{r_y}) &= E^n_{i,1}(2 - (C^2_{r_x} + C^2_{r_y}) - b - 2C^2_{r_y}\sigma_y) + C^2_{r_y}E^n_{i,2} \\ &+ \frac{1}{2}C^2_{r_x}(E^n_{i+1,1} + E^n_{i-1,1}) + E^{n-1}_{i,1}(a - 1 + A_r C_{r_y}) \\ E^{n+1}_{l_x/\Delta x,j}(1 + a + A_r C_{r_x}) &= E^n_{l_x/\Delta x,j}(2 - (C^2_{r_x} + C^2_{r_y}) - b - 2C^2_{r_x}\sigma_x) + C^2_{r_x}E^n_{l_x/\Delta x-1,j} \\ &+ \frac{1}{2}C^2_{r_y}(E^n_{l_x/\Delta x,j+1} + E^n_{l_x/\Delta x,j-1}) + E^{n-1}_{l_x/\Delta x,j}(a - 1 + A_r C_{r_x}) \\ E^{n+1}_{i,l_y/\Delta y}(1 + a + A_r C_{r_y}) &= E^n_{i,l_y/\Delta y}(2 - (C^2_{r_x} + C^2_{r_y}) - b - 2C^2_{r_y}\sigma_y) + C^2_{r_y}E^n_{i,l_y/\Delta y-1} \\ &+ \frac{1}{2}C^2_{r_x}(E^n_{i+1,l_y/\Delta y} + E^n_{i-1,l_y/\Delta y}) + E^{n-1}_{i,l_y/\Delta y}(a - 1 + A_r C_{r_y})\end{aligned}$$

with $\sigma_x = \frac{ArD\Delta x}{\lambda}$ and $\sigma_y = \frac{ArD\Delta y}{\lambda}$.

4.4 Stability

The maximum sizes allowed for the simulation steps Δt, Δx and Δy to avoid instabilities are now calculated by Von Neumann analysis. Assuming that the solution of Eq. (28) is given by:

$$E_{i,j}^n = Z^n e^{\mathbf{j}(\theta i + \omega j)} \tag{29}$$

where Z can be complex, but θ and ω are real, we define the amplification factor as $G = \frac{E_{i,j}^{n+1}}{E_{i,j}^n}$. The necessary condition for the solution to remain bounded is:

$$|G| \leq 1 \tag{30}$$

Substituting Eq. (29) in Eq. (28), we get:

$$\begin{aligned} Z^{n+1}e^{\mathbf{j}\theta i}e^{\mathbf{j}\omega j}(a+1) &= Z^{n-1}e^{\mathbf{j}\theta i}e^{\mathbf{j}\omega j}(a-1) \\ &+ Z^n e^{\mathbf{j}\theta i}e^{\mathbf{j}\omega j}(2 - C_{r_x}^2 - C_{r_y}^2 - b) \\ &+ \frac{1}{2}C_{r_x}^2(Z^n e^{\mathbf{j}\theta(i+1)}e^{\mathbf{j}\omega j} + Z^n e^{\mathbf{j}\theta(i-1)}e^{\mathbf{j}\omega j}) \\ &+ \frac{1}{2}C_{r_y}^2(Z^n e^{\mathbf{j}\theta i}e^{\mathbf{j}\omega(j+1)} + Z^n e^{\mathbf{j}\theta i}e^{\mathbf{j}\omega(j-1)}) \end{aligned}$$

with $Z^n(e^{\mathbf{j}\theta(i+1)}e^{\mathbf{j}\omega j} + e^{\mathbf{j}\theta(i-1)}e^{\mathbf{j}\omega j}) = 2Z^n e^{\mathbf{j}\omega j}\cos(\theta) = 2Z^n e^{\mathbf{j}\omega j}(1 - 2\sin^2(\frac{\theta}{2}))$ and dividing by $Z^{n-1}e^{\mathbf{j}\theta i}e^{\mathbf{j}\omega j}$, we get:

$$Z^2(1+a) - Z\epsilon + 1 - a = 0$$

where $\epsilon = 2 - b - 2(C_{r_x}^2 sin^2(\frac{\theta}{2}) + C_{r_y}^2 sin^2(\frac{\omega}{2}))$. This is a second degree equation with solutions depending on the sign of the discriminant $\Delta = \epsilon^2 - 4(1-a^2)$.

- If $\Delta > 0$

  $$Z_{\Delta>0} = \frac{\epsilon \pm \sqrt{\Delta}}{2(1+a)}$$

  The stability condition Eq. (30) reduces to:

  $$\left|\frac{\epsilon \pm \sqrt{\Delta}}{2(1+a)}\right| < 1$$

  From the triangle inequality, $|\epsilon| + |\sqrt{\Delta}|$ is an upper bound of $|\epsilon + \sqrt{\Delta}|$. With $\Delta > 0$ and $2(1+a) > 0$, a sufficient stability condition is given by:

  $$\frac{|\epsilon| + \sqrt{\Delta}}{2(1+a)} < 1$$

  that is, $|\epsilon| < 2$. Indeed, in this case, $\Delta = 4a^2 - (4 - \epsilon^2) \leq 4a^2$ and $\sqrt{\Delta} \leq 2a$.
  Replacing by $\epsilon = 2 - b - 2(C_{r_x}^2 + C_{r_y}^2)sin^2(\frac{\theta}{2})$ and $b = AD(\frac{c\Delta t}{\lambda})^2$, we obtain two conditions:

  $$\epsilon < 2, \quad b + 2(C_{r_x}^2 sin^2(\frac{\theta}{2}) + C_{r_y}^2 sin^2(\frac{\omega}{2}) > 0$$

  and:

  $$\epsilon > -2, \quad (C_{r_x}^2 sin^2(\frac{\theta}{2}) + C_{r_y}^2 sin^2(\frac{\omega}{2}) < 2 - \frac{b}{2}$$

  The first condition is always satisfied because $b = AD\left(\frac{c\Delta t}{2\lambda}\right)^2 > 0$. The second is obtained by taking the upper bounds of $sin^2(\frac{\theta}{2})$ and $sin^2(\frac{\omega}{2})$ equal to 1. Realizing then that:

  $$b = AD\left(\frac{c\Delta t}{2\lambda}\right)^2 = C_{r_x}^2 AD(\frac{\Delta x}{2\lambda})^2 = C_{r_y}^2 AD(\frac{\Delta y}{2\lambda})^2$$

we obtain the stability condition for the parameters of the FDTD model:

$$C_{r_x}^2(1+AD(\frac{\Delta x}{2\lambda})^2)+C_{r_y}^2(1+AD(\frac{\Delta y}{2\lambda})^2)<2 \tag{31}$$

which is satisfied if both conditions $C_{r_x}^2(1+AD(\frac{\Delta x}{2\lambda})^2)<1$ and $C_{r_y}^2(1+AD(\frac{\Delta y}{2\lambda})^2)<1$ are simultaneously satisfied.

- If $\Delta<0$

$$Z_{\Delta<0}=\frac{\epsilon\pm\mathbf{j}\sqrt{-\Delta}}{2(1+a)}$$

where $\mathbf{j}=\sqrt{-1}$. As previously, stability is given by Eq. (30):

$$\left|\frac{\epsilon\pm\mathbf{j}\sqrt{-\Delta}}{2(1+a)}\right|<1$$

As the module of a complex number $z=x+\mathbf{j}y$ is given by $|x+\mathbf{j}y|=\sqrt{x^2+y^2}$, we have:

$$\frac{\epsilon^2-\Delta}{4(1+a)^2}<1$$

Replacing Δ by its value, we obtain:

$$\frac{4(1-a^2)}{4(1+a)^2}=\frac{1-a}{1+a}<1$$

This condition is always fulfilled.

We conclude that as long as $\Delta<0$, the schemes are unconditionally stable. If $\Delta>0$, stability condition (31) must be respected. The stability condition involves the absorption and scattering coefficients, the mean free path and the time and space discretization steps. We therefore study the domains of variation of those parameters for stability.

To start with, the space discretization steps Δx and Δy do not have to be small as we are studying energy propagation. We set them at $\Delta x=\Delta y=1$m. Inversely, if the time discretization step is small, results will be precise. We choose values for the absorption and scattering coefficient between 0.1 and 0.9, and 0.1 and 1.9 respectively. And we set the mean free path to 5.4m and the speed of sound to 344m/s. Table 1 gives the maximum values of Δt for the model to remain stable, as computed from Eq. (31).

Table 1: Maximum values of Δt to respect the stability condition as function of the model parameters α, β. Other parameters are fixed to $\Delta x=\Delta y=1$m, $c=344$m/s and $\lambda=5.4$m.

α	β	$\Delta t(ms)$
0.1	0.1	2.91
	1.1	2.90
	1.9	2.88
0.5	0.1	2.91
	1.1	2.89
	1.9	2.70
0.9	0.1	2.91
	1.1	2.88
	1.9	2.46

The stability condition is not sensitive to variations of the absorption and scattering coefficients, except for large scattering. This is because the terms $AD(\frac{\Delta x}{2\lambda})^2$ and $AD(\frac{\Delta y}{2\lambda})^2$ in the stability condition (31) are much smaller that 1 except for large values of β.

5 Applications

To assess the general equation, we compute the model with MATLAB. The computation results are first validated by varying the absorption and scattering coefficients. Then, we compare the results with *in situ* measurements. This permits to obtain the coefficients by an adjustment procedure. We present energy levels after time integration for each position of receiver (space decays), and as function of time after source extinction for two receiver positions (time decays).

5.1 Computation results

5.1.1 Model parameters

The FDTD model is calculated for an impulsive source of 100dB sending sound energy through a *quasi*-infinite 200m by 200m room. The source is situated in the centre of the room, 100m from all walls, and receivers are positioned every meter from the source along one of the axes. The values of the absorption and scattering coefficients are set from $\alpha = 0.01$ to $\alpha = 0.8$ and from $\beta = 0.01$ to $\beta = 1.5$. The absorption coefficients on all sides are set to $\alpha_r = \alpha$, that is, $A_r = A/4$. The mean free path is $\lambda = 5.4$m and corresponds to the mean free path of the open spaces measured in Sec. 5.2. The space and time discretization steps are set to $\Delta x = \Delta y = 1$m, $\Delta t = 1.10^{-3}$s. The speed of sound is $c = 344$m/s.

5.1.2 Space decays

To begin with, Fig. 1 plots the (steady-state) energy space decays for different values of the absorption and scattering coefficients.

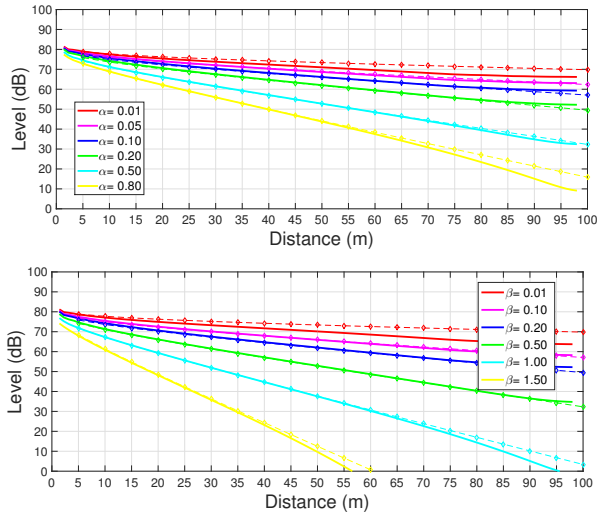

Figure 1: Energy space decays for different values of α (upper pane, with $\beta = 0.2$ and α taking values 0.01, 0.05, 0.1, 0.2, 0.5 and 0.8 from top to bottom) and β (lower pane, with $\alpha = 0.2$ and β taking values 0.01, 0.1, 0.2, 0.5, 1. and 1.5 from top to bottom) in a 200m by 200m *quasi*-infinite room with the source in the middle of the room. Receivers are positioned along one axis. Parameters are set to $\lambda = 5.4$m, $\Delta x = \Delta y = 1$m, $\Delta t = 1$ms and $\alpha_r = \alpha$ on all sides. Lozenges correspond to the Bessel solution of Eq. (22), with $E_0 = 74$dB (colour on-line).

The increase of the slope of the space decays in Fig. 1 is clearly visible as α or β increases. One can observe that energy stays around the source for large values of α or β, leading to a decrease of energy with distance. Measurement of the decay rates in Fig. 1 gives values varying in the top pane from 0.15dB/m for $\alpha = 0.01$ to 0.6dB/m for $\alpha = 0.8$; and in the bottom pane, varying from 0.16dB/m for $\beta = 0.01$ to 1.3dB/m for $\beta = 1.5$. These decay rates are similar to the results obtained in the one-dimensional case; and they correspond to the values expected from Eq. (22), with the

same $E_0 = 74$dB in all cases, except for very small values of the parameters or for large distances. In the later cases, computed decays are systematically larger than their analytical approximations.

5.1.3 Time decays

Secondly, Fig. 2 and 3 plot the energy time decays for different values of the absorption and scattering coefficients.

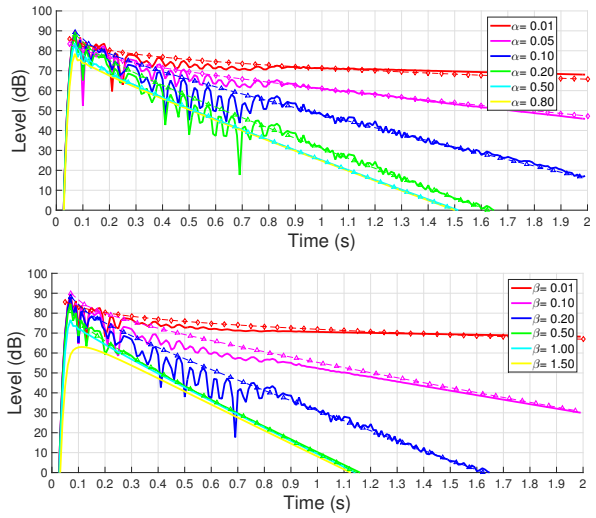

Figure 2: Energy time decays at 15m from the source for different values of α (upper pane, same parameters as in Fig. 1) and β (lower pane, same parameters as in Fig. 1) in a 200m by 200m *quasi*-infinite room with the source in the middle of the room and the receiver position at $r = 15$m from the source along one axis. Parameters are set to $\lambda = 5.4$m, $\Delta x = \Delta y = 1$m, $\Delta t = 1$ms and $\alpha_r = \alpha$ on all sides. Lozenges correspond to Eq. (24) and triangles to Eq. (25) (colour on-line).

As for the space decays, the slope of the time decays at 15m from the source is increasing as α or β increases as long as the varying parameter is smaller than the fixed one: beyond this value, which corresponds to $D = \frac{3}{4}A$, slopes remain constant but levels decrease, as proven by the comparisons with Eq. (25). In other words, the smaller of the two absorption and scattering coefficients pilots the time decays, as in the one-dimensional case [8]. Measurement of the decay rates gives values varying in the top pane from 3.3dB/s for $\alpha = 0.01$ to 50dB/s for $\alpha \geq 0.2$; and in the bottom pane, varying from 2.5dB/s for $\beta = 0.01$ to 65dB/s for $\beta \geq 0.5$.

Compared to space decays, the first halves of the time decays display large oscillations which gradually fade away in the second halves; however, for large values of α in the upper pane, and large values of β in the lower pane, oscillations disappear. For large differences between β and α, the decay is piloted by a diffusion equation, with solution given by Eq. (24) and $E_1 = 74$dB: this is the case for $\alpha = 0.01$ and $\alpha = 0.05$ when $\beta = 0.2$, and $\beta = 0.01$ when $\alpha = 0.2$. Notice that the approximate solution Eq. (25), where A is replaced by the smaller of the two coefficients A and D, correctly reflects the "arrival time" of the signal at $t_{max} = \sqrt{2}r/c$, and the maximum level prior to decay, with $E_2 = 101$dB except for the largest values of α and β where $E_2 = 95$dB.

It should also be noticed in both panes that the approximate diffusion equation predicts energy before the "arrival time" of the signals, due to the absence of the second time derivative in the corresponding equation; and that it does not correspond well to the decay for $\beta = 0.1$ in the bottom pane, because β is no longer small with respect to α. This shows the limits of the diffusion approximation.

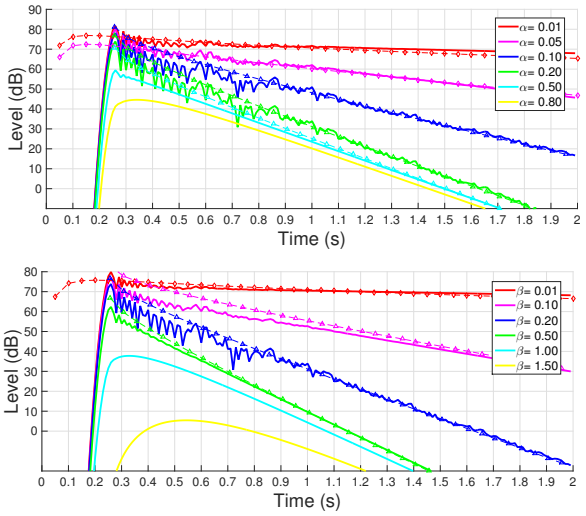

Figure 3: Energy time decays at 60m from the source for different values of α (upper pane, same parameters as in Fig. 1) and β (lower pane, same parameters as in Fig. 1) in a 200m by 200m *quasi*-infinite room with the source in the middle of the room and the receiver position at $r = 60$m from the source along one axis. Parameters are set to $\lambda = 5.4$m, $\Delta x = \Delta y = 1$m, $\Delta t = 1$ms and $\alpha_r = \alpha$ on all sides. Lozenges correspond to Eq. (24) and triangles to Eq. (25) (colour on-line).

At 60m from the source, like at 15m, the time decay slopes increase when α or β increases. The same trends as observed at 15m survive at this larger distance: same oscillations; same stabilizing factors; same values of the coefficients for maximum decays, with same behaviours of the plots, leading to the same conclusion that decays are piloted by the smaller of the two coefficients A and D.

Decay rates in the upper pane ($\beta = 0.2$) range from 3.5dB/s for $\alpha = 0.01$ to 50dB/s for $\alpha = 0.8$; and in the bottom pane ($\alpha = 0.2$) from 2.3dB/s for $\beta = 0.01$ to 65dB/s for $\beta = 1.5$. Detailed comparison shows that they take the same values as at 15m from the source. Once again, oscillations appear in the first half of the decays for small values of α or β. One can also observe that at this distance, the maximum levels of the decays decrease when the coefficients increase. Similarly, the arrival times of the maxima increase when the distance increase; but the maxima are never attained before the arrivals of the direct sounds at $t_{max} = \sqrt{2}r/c$, as given by Eq. (25). Once again, the approximate diffusion equation predicts energy before the "arrival time" of the signals and is not very accurate even for the lowest values of α and β. As for the adjustment factors E_1 and E_2 of the approximate solutions, they take the same values as at 15m for corresponding parameters.

Further, as predicted in Sec. 3.4, Fig. 4 shows that the diffusion solution becomes accurate beyond the arrival time of the signals when one of the parameters is very small with regards to the other one. The adjustment factor E_1 takes the value 71dB for $\alpha = 0.01$ and $\beta = 1.5$, and 70dB for $\alpha = 0.8$ and $\beta = 0.01$.

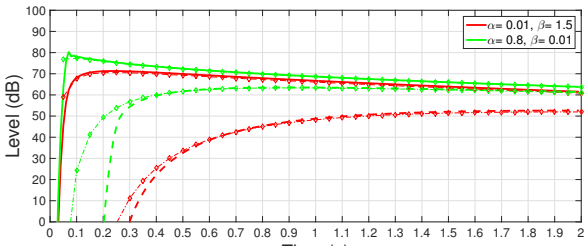

Figure 4: Energy time decays for negligible values of one parameter with respect to the other in the same 200m by 200m *quasi*-infinite room with the source in the middle of the room. Receiver position is either 15m (continuous lines) or 60m (broken lines) from the source along one axis. From top to bottom, parameters are: $\alpha = 0.8$ and $\beta = 0.01$, receiver at 15m; $\alpha = 0.01$ and $\beta = 1.5$, receiver at 15m; $\alpha = 0.8$ and $\beta = 0.01$, receiver at 60m; $\alpha = 0.01$ and $\beta = 1.5$, receiver at 60m. The other parameters are set to $\lambda = 5.4$m, $\Delta x = \Delta y = 1$m, $\Delta t = 1$ms and $\alpha_r = \alpha$ on all sides. Lozenges correspond to Eq. (24) (colour on-line).

5.2 Comparison with measurements

5.2.1 Measurements

Measurements have been made with the help of a *SoundField* ST250 microphone [16]. It is composed of four probes in tetrahedral array from which one can recover the pressure at the central position, and the pressure gradient along the three Cartesian axes. The sound source was an *Outline* GRS omnidirectional speaker constituted of twelve speakers and a *Tannoy* VS10 subwoofer. We used a *MOTU*®Traveler sound card and a laptop with *Adobe Audition* software and Aurora plug-in to both send and record the signals. The measuring signal is a 20Hz to 20kHz, 10s sweep sine. Signals recorded were post-treated to obtain room impulse responses by convolution with the inverse sweep. The Outline source was positioned 1.5m above the floor, with the subwoofer on the floor below it.

5.2.2 Rooms characteristics

Measurements were carried out in two open-offices in Paris. One of them was empty, and the other one furnished. Systematic measurements with distance were carried out only in the furnished office; but the empty offices was large enough to allow a limited set of measurements at distance up to 20m from the source which are presented here.

- Kaleido is a 23m long and 20m wide open-office of 300m^2, 2.7m high, with a mean free path of 5.4m according to Eq. (11). The floor is made of soft carpet, the ceiling is constituted of mineral wool panels and the walls are windows and plaster. There was no furniture the days of the measurement, and the room was empty, except for 12 structural columns regularly distributed in the room. A plan of Kaleido is displayed in the top pane of Fig. 5.

- Ovalie is a 75m long by 35m wide open-office with oval shape and a central island. Its area is 1260m^2, and its hight 2.7m, leading to a mean free path of 5.4m according to Eq. (11). The room features are soft carpet on the floor and compact mineral wool panels on the ceiling. The walls are made of windows and plaster. Moreover, the room is furnished with equipments such as desks, chairs, computers, and other equipments needed for normal operation; but measurements were made in absence of the users. A plan of Ovalie is displayed in the bottom pane of Fig. 5.

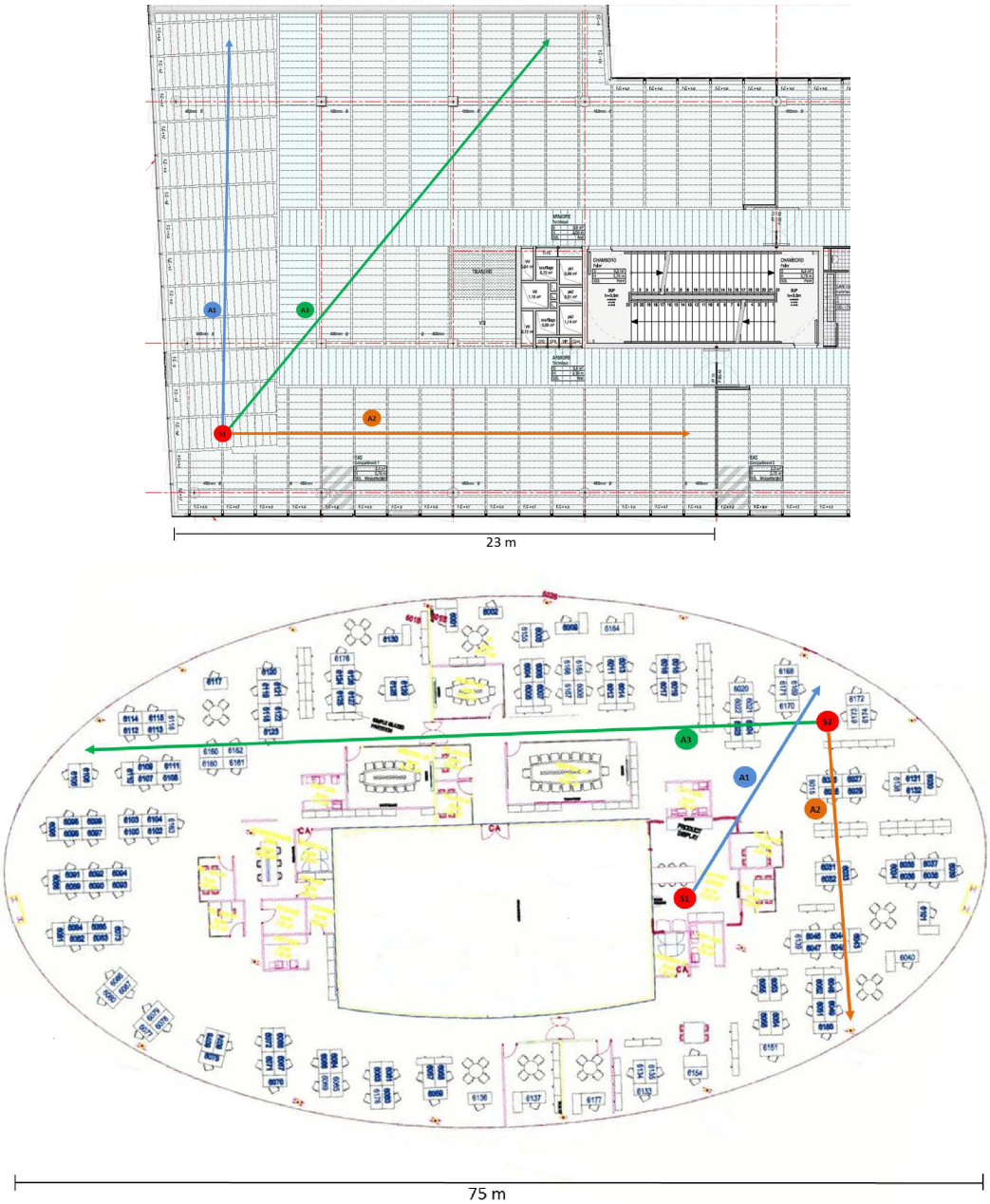

Figure 5: Plans of the rooms under measurement: Kaleido in top pane, and Ovalie in the bottom pane. The source positions are shown by red circles and the 3 axes of measurement for each rooms by blue, orange and green arrows (colour on-line).

.

5.2.3 Adjustment procedure

Estimations of the absorption and scattering coefficients can be derived from comparison with measurements. We saw above in Sec. 5.1.3 that for values of β larger than α, variations of β do not influence the slope of the time decay. Thus, an iterative procedure has been used to estimate α and β by first assuming β to be large and estimating the absorption coefficients from time decays, then deducing β with the help of the space decays. The procedure, however, exaggerates the slopes, both for time and space decay, so the coefficients are marginally adjusted for a better fit.

Fig. 6 plots two time decays (top panes) for the 1kHz octave band in Kaleido, with the simulated decay for the adjusted absorption coefficient. The space decay (bottom pane) gives the scattering

coefficients in the 1kHz octave band. α and β are respectively 0.16 and 1.2, both at 4m (top left pane) and 16m (top right pane) from the source, which in this case is S3 (see Fig. 5). Notice the double slopes of the time decays, and that the absorption coefficient is adjusted on the second slope. The arrival time is adjusted on the maximum of the decays, but the overall level is overestimated by the simulation. This overestimation is also visible on the space decay (bottom pane).

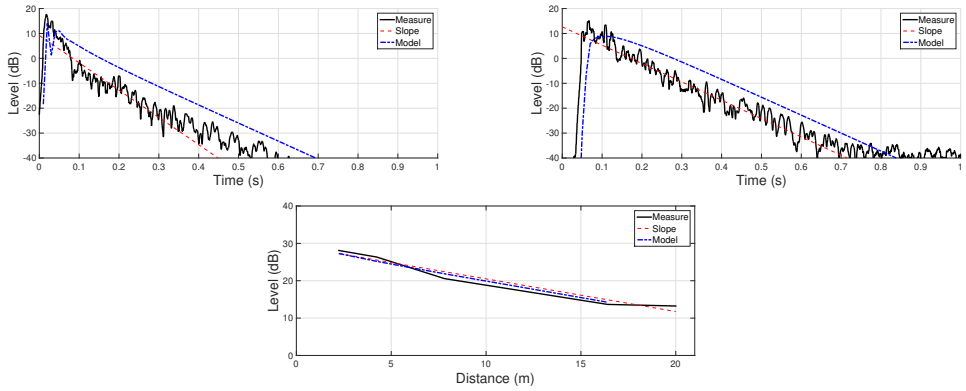

Figure 6: Adjustment of the model by comparison with the time decays measured at 4m from the source (top left pane) and at 16m from the source (top right pane), and with the space decay (bottom pane), in the room Kaleido. Source 3, $\alpha = 0.16$ and $\beta = 1.2$ (colour on-line).

Fig. 7 plots time decays (top panes) for the 1kHz octave band in Ovalie, with the simulated decay for the adjusted absorption coefficient. The space decay (bottom pane) gives the scattering coefficients in the 1kHz octave band. α and β are respectively 0.21 and 0.7, both at 10m (top left pane) and 40m (top right pane) from the source which in this case is S3 (see Fig. 5). Again, double slopes are visible in the time decays, and the simulation overestimates the levels. Notice that the earlier space decay can no longer be considered as linear with distance: in fact, a logarithmic plot shows that the decay follows a power law up to about 15m from the source, corresponding to the influence of the direct sound, but not beyond that distance; but the overestimation of the level by the simulation masks the importance of the direct sound. Also notice the drop in level beyond 20m, which corresponds to a door visible on Fig. 5.

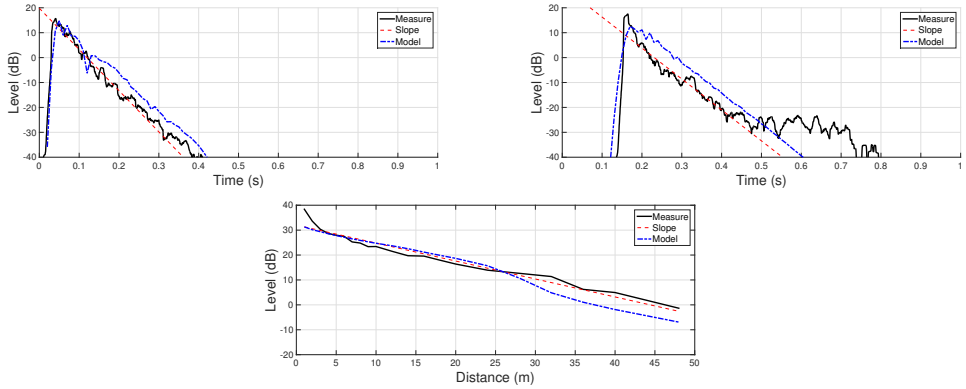

Figure 7: Adjustment of the model by comparison with the time and space decays measured at 10m from source (left panes) and at 40m from the source (right panes), and with the space decay (bottom pane), in the room Ovalie. Source 3, $\alpha = 0.21$ and $\beta = 0.7$ (colour on-line).

But for the overestimation of the levels, simulations closely follow the time decays, and accurately the slope of the space decays except at large distances.

5.2.4 Comparison with Sabine formula

Using Sabine's formula (see Sec. 2.2) makes it possible to compute α from reverberation time measurements as:

$$\alpha = \frac{0.16V}{TS}$$

- in Kaleido the reverberation time is $T = 0.9$s. With $V = 1168\text{m}^3$ and $S = 1150\text{m}^2$, $\alpha = 0.18$, not far from $\alpha = 0.16$ obtained above in Sec. 5.2.3.
- in Ovalie the reverberation time is $T = 0.45$s . That is, with $V = 3407\text{m}^3$ and $S = 3789\text{m}^2$, $\alpha = 0.32$, compared to $\alpha = 0.21$ obtained above.

It must however be emphasized that Ovalie was furnished and partly partitioned when the measurements were taken (see Fig. 5), which explains the strong difference with Sabine's formula. On the other hand, Kaleido was empty.

6 Discussion

6.1 Adjustment procedure

The adjustment gives quite good results, as shown by Figs. 6 and 7, and also are in good agreement with the Sabine formula in the case of Kaleido. However, the approximate solutions Eqs. (24) and (25) give too slow time decays, even though the space decays are well approximated by the modified Bessel function solution of Eq. (22). This has to do with the proximity of the side walls in all measurements. Indeed, even in the case of the *quasi*-infinite room of Sec. 5.1, we obtained bad agreement between time decays and approximate solutions for sources and receivers in the proximity of a side wall. Thus, the proximity of a side wall reduces reverberation, confirming that reverberation measurements are not sufficient to characterize flat rooms, as stated in the Introduction.

6.2 Time of arrival of the direct sound

Figs. 2 and 3 show different times of arrival of the energy. Fig. 2 was calculated at 15m from the source and Fig. 3 at 60m, which gives times of arrival of the direct sound of resp. 44ms and 174ms. However, the arrival time of the signal is larger by a factor $\sqrt{2} = 1.4$, reflecting the slower speed of diffuse sound energy as stated in Secs. 3.4 and 5.1.3. This delay has been introduced in the upper panes of Figs. 2 and 3, as the measuring equipment does not conserve the propagation delay between the source and the receiver.

It should be stressed that the general equation (21) is not valid for the direct sound. The reason is that considerations of energy conservation led us to introduce a factor $1/2$ for the diagonal components of the wave-stress tensor $\underline{\underline{E}}$ in Sec. 3.3.3. This is not valid for the direct sound, as only one direction carries the whole energy, thus ensuring conservation of energy. How does the direct wave front convert to diffuse energy equally distributed in all directions is not further investigated in this paper: it involves more complex boundary conditions than what is described in Sec. 3.3.1 and 3.3.2, which are akin to the usual diffuse-field scattering coefficients on the walls (see e.g. [17, 18]). As a consequence, the scattering of the direct sound is not accounted for by the present model.

As for the approximate analytical solutions of Sec. 3.4, only the second one, Eq. (25), accounts for an arrival time of the diffuse energy, but not for the arrival time of the direct sound which must be handled separately. The diffusion solution (24) does not account for a finite speed of sound, with the result seen on Figs. 2, 3 and 4 that it predicts signal before the proper arrival time. Thus, Eq. (24) is not valid for time shorter than the arrival times; but for times just a little longer that the arrival time, Figs. 2, 3 and 4 prove that the approximation is acceptable.

6.3 Asymptotic space decay

As stated in the Introduction, ISO 14257:2001 standard [3] recommends to measure the energy decay with distance, and the praxis of consultant is therefore to measure the slope of the log-log

plot of decay with distance, assuming it to remain in the vicinity of the direct sound decay. In fact, this is only valid if the line of sight from source to receivers is not blocked, as stated by Kurze [19].

Moreover, Kurze gives several shapes of dependence of sound pressure with distance in his Fig. 1: for fitted flat rooms, decays are similar to the present model. Kuttruff [20] used his own radiosity model to derive a simplified model of energy propagation in flat rooms, the main feature of it, besides taking into account the direct sound, being a power law of exponent -3 for the late diffuse field decay; however, Kuttruff does not compare his computation with actual measurements. Here, we show, both computationally and experimentally, that this decay is asymptotically exponential, but for a factor inversely proportional to the square root of the distance.

As a consequence, we recommend to measure attenuation in flat rooms both along a line of sight of the source, as recommended by ISO 14257:2001 and [19], but also along other lines. Indeed, in a line of sight, the slow decay of the direct sound eventually dominates the measurements at very long distances. Measuring along blocked-sight lines is the only way to check whether the decays are fast (exponential but for the factor $1/\sqrt{r}$) as in long rooms, or slow (power law) as in [20].

7 Conclusion

In this paper, we have shown that the conservation of energy in a given volume consists of two equations: the conservation of the total energy; and the conservation of sound intensity. The two equations combine in a single tensor equation, the conservation of the stress-energy tensor.

In two dimensions, just like in one dimension, absorption and scattering on the boundaries modify these conservation equations. Combining this system of two equations into a single Telegraph equation involving energy only, the present paper develops a finite difference scheme to solve it. The scheme is stable, with the same stability conditions as in the one-dimensional case, and simulations using it have been compared to asymptotic expressions in the case of an infinite flat room. Systematic variations of the absorption or scattering coefficient while retaining the other coefficient constant shows the symmetric rôle played by the two coefficients: the smaller coefficient pilots time decays, and the larger is then obtained from space decay. However, an improved energy balance on the boundaries shows that the expressions of the modified absorption and scattering coefficient are not completely symmetrical, with a factor $3/4$ introduced in the scattering coefficient.

It turns out that the smaller coefficient usually is the absorption coefficient. Thus the absorption coefficient is obtained from the time decay curves; and the scattering coefficient from the space decay curve. This leads to the same adjustment procedure for evaluating absorption and scattering coefficients from measurement as was developed in one-dimension. The procedure was validated by comparing simulations with actual measurements in two open space offices, and permits to obtain good agreement. It should be noted that the adjustment can be local, that is, the procedure permits the evaluation of locally varying absorption and scattering coefficients. But in the present cases, global coefficients gave satisfactory results.

However, compared to the one-dimensional case, new hypotheses must be introduced to solve the two-dimensional case. Here, we opt for the isotropy of the sound energy, but do not dwell on the transition from the unidirectional direct sound to the isotropic diffuse sound. This transition will be the object of future work. Future work must also experimentally check the fast decay of the sound field with distance when the direct sound is blocked.

8 Appendix: Energy distribution function

In Secs. 3.3.1 and 3.3.2, we introduced the energy distribution function $f(\vec{r}, \vec{v}, t)$ that describes the probability that a sound wave at position $\vec{r}$ travels in the direction $\vec{v}$ at time t. We here justify the formalism used in those two Sections.

8.1 Energy distribution

The concept of energy distribution arises within a sound field when it is composed of many sound waves travelling in all directions. This is typically the case of the reverberant or diffuse sound fields where the waves carry roughly the same amount of energy, that is, the energy is nearly isotropically

distributed. As a consequence, the central limit theorem applies and the energy distribution is characterized by its moments of the direction cosines up to the order two.

More specifically, realizing that the expansion proposed by [9] makes uses of the spherical harmonics of degree 0 and 1, we expand the energy distribution function one degree further. Indeed, the spherical harmonics constitute a complete set of orthogonal functions on the sphere; and the truncation at degree 2 is consistent with the above remark on the highest moments to be considered, even though the expansion does not use the direction cosines but the spherical angular coordinates θ and ϕ, where θ is the angle with the vertical direction z and ϕ the angle in the horizontal plane with respect to the x-axis. Thus, the energy distribution function f is defined as:

$$f(\vec{r},\vec{v},t) = \frac{E}{4\pi} + \frac{3\vec{J}}{4\pi}\cdot\frac{\vec{v}}{c} + \frac{5}{4\pi}\left\{\begin{array}{c} \frac{1}{4}(2E_{zz}-E_{xx}-E_{yy})(3\cos^2\theta-1) \\ +3E_{xz}\cos\theta\sin\theta\cos\phi + 3E_{yz}\cos\theta\sin\theta\sin\phi \\ +\frac{3}{4}(E_{xx}-E_{yy})\sin^2\theta\cos 2\phi + \frac{3}{4}E_{xy}\sin^2\theta\sin 2\phi \end{array}\right\}$$

It should be noticed that this definition makes use of the fact that the Hamiltonian

$$H = \frac{\rho}{2}(-\frac{1}{c^2}|\partial_t\Psi|^2 + |\vec{\nabla}\Psi|^2)$$

vanishes in the volume, that is,

$$E - E_{xx} - E_{yy} - E_{zz} = 0$$

in the volume. This hypothesis is consistent with a sound field composed of many sound waves, as waves naturally have a vanishing Hamiltonian. We thus recover by integration on the whole solid angle $\Omega = (\theta,\phi)$ with $\theta\in[0,\pi]$, $\phi\in[0,2\pi]$:

$$\begin{aligned}
&\int_\Omega f(\vec{r},\vec{v},t)d\Omega = \int_0^{2\pi}\int_0^{\pi} f(\vec{r},\vec{v},t)\cos\theta\sin\theta d\theta d\phi = E \\
&\int_\Omega f(\vec{r},\vec{v},t)\sin^2\theta\cos^2\phi d\Omega = E_{xx} \\
&\int_\Omega f(\vec{r},\vec{v},t)\sin^2\theta\sin^2\phi d\Omega = E_{yy} \\
&\int_\Omega f(\vec{r},\vec{v},t)\cos^2\theta d\Omega = E_{zz}
\end{aligned}$$

Similar integrations lead to the sound intensity $\vec{J}$ and the wave-stress elements E_{xy}, E_{xz} and E_{yz}. Note that $f(\vec{r},\vec{v},t)$ is not a probability density, as it is not normalized to unity, but to the total energy, as proven by the first equation above.

8.2 Energy balance on walls

With the use of the energy distribution function, energy balance can be computed on each wall. For example, the incident energy locally entering the ceiling is then obtained by integrating the vertical component of the flux, $f(\vec{r},\vec{v},t)\vec{v}$ over the solid angle $\Omega = (\theta,\phi)$ with $\theta\in[0,\frac{\pi}{2}]$, $\phi\in[0,2\pi]$:

$$\begin{aligned}
J_{z,inc} &= \int_\Omega f(\vec{r},\vec{v},t)\frac{\vec{v}}{c}\cdot\vec{n}d\Omega \\
&= \int_0^{2\pi}\int_0^{\frac{\pi}{2}} f(\vec{r},\vec{v},t)\cos\theta\sin\theta d\theta d\phi \\
&= \frac{E}{4} + \frac{J_z}{2} + \frac{5}{32}(2E_{zz}-E_{xx}-E_{yy})
\end{aligned}$$

Similarly, the reflected energy is given by integrating over the solid angle $\Omega' = (\theta,\phi)$ with $\theta\in[\frac{\pi}{2},\pi]$, $\phi\in[0,2\pi]$:

$$J_{z,ref} = \frac{E}{4} - \frac{J_z}{2} + \frac{5}{32}(2E_{zz}-E_{xx}-E_{yy})$$

The absorbed energy is then obtained as the difference between incident and reflected energies, that is:

$$J_{z,inc} - J_{z,ref} = J_{z,abs} = J_z$$

Introducing the Sabine absorption coefficient α as the ratio of absorbed energy flow to incident energy flow, the sound intensity absorbed by the ceiling becomes:

$$J_{z,abs} = J_z = \alpha J_{z,inc} = \alpha \left\{ \frac{E}{4} + \frac{J_z}{2} + \frac{5}{32}(2E_{zz} - E_{xx} - E_{yy}) \right\}$$

that is:

$$J_{z,abs} = \frac{\alpha}{2(2-\alpha)} \left\{ E + \frac{5}{8}(2E_{zz} - E_{xx} - E_{yy}) \right\}$$

Thus, the absorbed energy is not just proportional the total energy in front of the ceiling, but includes a term proportional to the deviation $(2E_{zz} - E_{yy} - E_{xx})$ of the energy repartition from a perfectly diffuse field. Similar expression are obtained for the floor as well as all the other walls.

8.3 Momentum balance on walls

Stress momentum balance on the walls is computed similarly by integration on the same solid angles Ω and Ω'. The stress momentum $M_{xz,in}$ going into the ceiling thus becomes:

$$\begin{aligned} M_{xz,in} &= \int_{\Omega} f(\sin\theta\cos\phi)\frac{\vec{v}\cdot\vec{n}}{c}d\Omega \\ &= \int_0^{2\pi}\int_0^{\frac{\pi}{2}} f(\vec{r},\vec{v},t)(\sin\theta\cos\phi\cos\theta)\sin\theta d\theta d\phi \\ &= \frac{3}{16}J_x + \frac{1}{2}E_{xz} \end{aligned}$$

where $\sin\theta\cos\phi$ is a spherical harmonic of order 1; and the stress momentum $M_{xz,out}$ going out of the wall is:

$$\begin{aligned} M_{xz,out} &= -\int_{\Omega'} f(\sin\theta\cos\phi)\frac{\vec{v}\cdot\vec{n}}{c}d\Omega \\ &= -\int_0^{2\pi}\int_{\frac{\pi}{2}}^{\pi} f(\vec{r},\vec{v},t)(\sin\theta\cos\phi\cos\theta)\sin\theta d\theta d\phi \\ &= \frac{3}{16}J_x - \frac{1}{2}E_{xz} \end{aligned}$$

The scattered momentum is then obtained as the difference between incoming and outgoing momenta, that is:

$$M_{xz,in} - M_{xz,out} = M_{xz,scat} = E_{xz} \tag{32}$$

Introducing a scattering coefficient β as the ration of scattered momentum to incoming momentum, the momentum scattered by the ceiling becomes:

$$M_{xz,scat} = E_{xz} = \beta M_{xz,in} = \beta\left(\frac{3J_x}{16} + \frac{E_{xz}}{2}\right)$$

that is:

$$E_{xz} = \frac{3}{4}\frac{\beta}{2(2-\beta)}J_x$$

In other words, the wave stress component E_{xz} in just in front of the ceiling is proportional to the sound intensity J_x which flows parallel to the ceiling. Similar expressions are obtained for the wave stress component E_{yz}, and on the floor. The same results hold for the other walls for the corresponding wave stress components.

8.4 Discussion

In Secs. 3.3.1 and 3.3.2, we assumed that E, E_{xx} and E_{yy} are independent of the vertical coordinate z. And in Sec. 3.3.3, we further assumed that $E_{xx} = E_{yy} = \frac{E}{2}$. This means that E_{zz} vanishes in the flat room, reducing the energy balance to:

$$\begin{aligned} J_{z,abs} &= \frac{\alpha}{2(2-\alpha)} \left\{ E + \frac{5}{8}(2E_{zz} - E_{yy} - E_{xx}) \right\} \\ &= \frac{\alpha}{2(2-\alpha)} \left\{ E - \frac{5}{8}E \right\} = \frac{\alpha}{2(2-\alpha)} \frac{3}{8} E \end{aligned} \tag{33}$$

Compared to the relation derived by Jing and Xiang [12]:

$$J_{z,abs} = \frac{\alpha}{2(2-\alpha)} E \tag{34}$$

Eq. (33) displays a reduced efficiency of the absorption coefficients on the ceiling and the floor, by a factor somewhat less than one half. This seems logical as the majority of rays impinging on the ceiling and the floor of a flat room arrive at grazing incidence.

On the other hand, one can expect a redistribution of energy directions in the vicinity of the ceiling and the floor, as energy does flow into them when they are absorbing. At most, one expects an even distribution of energy in all directions, leading to a vanishing deviation $(2E_{zz} - E_{yy} - E_{xx}) = 0$. In this case, Jin and Xiang relation (34) holds.

There is, therefore, a need for experimental evaluation of the energy balance in the vicinity of the walls, along the line sketched in [21], in order to decide which of the two Eqs. (33) and (34) corresponds to the energy balance on the boundaries. In the absence of decisive evidence, we opt for the traditional balance Eq. (34), which has been used in this paper.

Acknowledgement

This work was carried out under a CIFRE convention (n° 2012/1184) between Impédance S.A.S. and Université Pierre et Marie Curie (Institut Jean le Rond d'Alembert), thanks to a grant from ANRT. The authors thank Impédance for providing access to the open spaces measured in Sec. 5.2.

References

[1] W. Sabine, *Collected Papers on Acoustics*, ch. 1. Reverberation. Peninsula Publishing, 1993.

[2] J. Bosquet, "Théorie synthétique de la réverbération et quelques données expérimentales," *Bulletin du Laboratoire d'Electroacoustique, Université de Liège*, vol. 11, pp. 51–67, June 1967.

[3] "Acoustics – Measurement and parametric description of spatial sound distribution curves in workrooms for evaluation of their acoustical performance." ISO Standard 14257:2001, Oct. 2001.

[4] "Arrêté relatif à la correction acoustique des locaux de travail." Journal Officel de la République Française, September 1990.

[5] F. Ollendorff, "Statistical room acoustics as a problem of diffusion, a proposal," *Acustica*, vol. 21, pp. 236–245, 1969.

[6] J. Picaut, L. Simon, and J. D. Polack, "A mathematical model of diffuse sound field based on a diffusion equation," *Acta Acust united Ac*, vol. 83, no. 4, pp. 614–621, 1997.

[7] C. Foy, V. Valeau, A. Billon, J. Picaut, and A. Sakout, "An Empirical Diffusion Model for Acoustic Prediction in Rooms with Mixed Diffuse and Specular Reflections," *Acta Acust united Ac*, vol. 95, no. 1, pp. 97–105, 2009.

[8] H. Dujourdy, B. Pialot, T. Toulemonde, and J. Polack, "An Energetic Wave Equation for Modelling Diffuse Sound Fields – Application to Corridors," *Acta Acustica united with Austica*, vol. 103, p. 480 – 491, 2017.

[9] P. M. Morse and H. Feshbach, *Method of Theoretical Physics*. Mc Graw-Hill Book Company, 1953.

[10] P. M. Morse and K. U. Ingard, *Theoretical Acoustics*. Mc Graw-Hill Book Company, 1968.

[11] J.-D. Polack, *Acoustic Quality of Concert Halls*, ch. 2. Sound fields in rooms: an introduction to reverberation theory, pp. 27–61. Spanish Acoustical Society, 1995.

[12] Y. Jing and N. Xiang, "On boundary conditions for the diffusion equation in room acoustic prediction: theory, simulations, and experiments," *J. Acoust. Soc. Am.*, vol. 123, no. 1, pp. 145–153, 2008.

[13] V. Valeau, J. Picaut, and M. Hodgson, "On the use of a diffusion equation for room-acoustic prediction," *J. Acoust. Soc. Am.*, vol. 119, no. 3, pp. 1504–1513, 2006.

[14] M. Abramowitz and I. Stegun, *Handbook of Mathematical Functions*. Dover, New York, 9th ed., 1972.

[15] M. Bruneau, *Introduction aux théories de l'acoustique*. Université du Maine, 1983.

[16] J. P. Espitia Hurtado, H. Dujourdy, and J. D. Polack, "Caractérisation expérimentale du microphone SoundField ST250 pour la mesure de la diffusivité du champ sonore," in *12ème Congrès Français d'Acoustique (CFA)*, (Poitiers, France), pp. 795–801, 2014.

[17] T. Sakuma, Y. Kosaka, L. Geetere, and M. Vorlander, "Relationship between the scattering coefficients determined with coherent averaging and with directivity correlation," *Acta Acust united Ac*, vol. 95, no. 4, pp. 669–677, 2009.

[18] I. Schmich and N. Brousse, "In situ measurement methods for characterising sound diffusion," in *Proceedings of the International Symposium on Room Acoustics, ISRA*, (Melbourne, Australia), p. 7, 29-31 August 2010.

[19] U. Kurtze, *Encyclopedia of Acoustics*, vol. 3, ch. 95. Sound propagation in work spaces, pp. 1181–1187. John Wiley & Sons, 1997.

[20] H. Kuttruff, "Stationäre Schallausbreitung in Flachraümen," *Acustica*, vol. 57, pp. 62–70, 1985.

[21] J. Polack, H. Dujourdy, N. Xiang, and X. Bai, "Novel scattering coefficient for diffusely reflecting surfaces," in *174th Meeting of the Acoustical Society of America* (ASA, ed.), vol. 142, p. 2559, 2017.